Picosecond-scale Terahertz pulse characterization with field-effect transistors

Regensburger, S.; Winnerl, S.; Klopf, J. M.; Lu, H.; Gossard, A. C.; Preu, S.;

Originally published:

March 2019

IEEE Transactions on Terahertz Science and Technology 9(2019)3, 262-271

DOI: https://doi.org/10.1109/TTHZ.2019.2903630

Picosecond-scale Terahertz pulse characterization with field-effect transistors

Stefan Regensburger, Stephan Winnerl, J. Michael Klopf, Hong Lu, Arthur C. Gossard, and Sascha Preu

Abstract

Precise real-time detection of Terahertz pulses is a key requirement in Terahertz communication technology, non-destructive testing, and characterization of pulsed Terahertz sources. We experimentally evaluate the speed limits of Terahertz rectification in field-effect transistors using the example of pulses from a free-electron laser. We develop an improved model for the description of these Terahertz pulses and demonstrate its validity experimentally by comparison to spectroscopic data as well as to expectation values calculated from free-electron laser physics. The model in conjunction with the high speed of the detectors permits the detection of an exponential rise time of the pulses as short as 5 ps despite a post detection time constant of 11 and 14 ps for a large area and an antenna-coupled detector, respectively. This proves that field-effect transistors are excellent compact, room-temperature Terahertz detectors for applications requiring an intermediate frequency bandwidth of several tens of GHz.

Index Terms

Field Effect Transistor, HEMT, Plasma waves, Terahertz (THz), Free Electron Laser, Semiconductor detectors, Pulse measurements, Ultrafast optics, Laser cavity resonators

Manuscript received September 14^{th}, 2018. This work was supported by the Deutsche Forschungsgemeinschaft, Project PR1413/2-1 (LA-FET).
(Corresponding author: Stefan Regensburger.)
S. Regensburger, and S. Preu are with Technische Universität Darmstadt, Germany. (e-mail: regensburger@imp.tu-darmstadt.de)
S. Winnerl, and J. M. Klopf are with the Helmholtz Zentrum Dresden-Rossendorf, Germany.
H. Lu is with the University of Nanjing, China.
A. C. Gossard is with the University of California, Santa Barbara, USA.

Picosecond-scale Terahertz pulse characterization with field-effect transistors

Stefan Regensburger, Stephan Winnerl, J. Michael Klopf, Hong Lu, Arthur C. Gossard, and Sascha Preu

***Abstract*—Precise real-time detection of Terahertz pulses is a key requirement in Terahertz communication technology, non-destructive testing, and characterization of pulsed Terahertz sources. We experimentally evaluate the speed limits of Terahertz rectification in field-effect transistors using the example of pulses from a free-electron laser. We develop an improved model for the description of these Terahertz pulses and demonstrate its validity experimentally by comparison to spectroscopic data as well as to expectation values calculated from free-electron laser physics. The model in conjunction with the high speed of the detectors permits the detection of an exponential rise time of the pulses as short as 5 ps despite a post detection time constant of 11 and 14 ps for a large area and an antenna-coupled detector, respectively. This proves that field-effect transistors are excellent compact, room-temperature Terahertz detectors for applications requiring an intermediate frequency bandwidth of several tens of GHz.**

***Index Terms*—Field Effect Transistor, HEMT, Plasma waves, Terahertz (THz), Free Electron Laser, Semiconductor detectors, Pulse measurements, Ultrafast optics, Laser cavity resonators**

I. Introduction

FIELD-effect transistors (FETs) are able to rectify radiation well above their maximum frequency of oscillation and cut-off frequency [1]. Within the last decade the sensitivity of FETs for THz detection has been strongly improved. In the class of fast and compact THz detectors at room-temperature, FETs have become competitive to Schottky diodes. Narrow-band FETs reach noise equivalent powers (NEPs) in the 10 $\mathrm{pW}/\sqrt{\mathrm{Hz}}$ range at THz frequencies [2], [3]. For many applications, in particular communication and fast data acquisition, the speed of the detection process is of major interest [4]. The detection of single THz pulses, as well as their intensity finds application in non-destructive testing, e.g. for thickness measurements [5]. Experiments requiring ultra-short THz pulses benefit from or even rely on a precise and real-time measurement of the pulse shape and pulse width for the precise quantification of peak quantities. Pulse width and pulse shape of picosecond THz pulses can be measured using autocorrelation setups [6], [7] or also electro-optical sampling [8]–[11]. There are limitations though for both methods, such as long integration times for scanning type measurements. For THz systems with jitter and phase jumps such as free-electron lasers (FELs), those measurement techniques are inadequate as the timing and the pulse shape might even change during the measurement. An alternative approach is to record the spectrum of the pulse and then perform a Fourier transformation to obtain the pulse in the time domain. However, spectroscopic data are insufficient to derive the temporal pulse shape. A spectrometer only measures the intensity spectrum and does not give access to the spectral phase. The Heisenberg-Gabor limit only allows to specify a lower boundary of the pulse width. The Fourier transform of spectroscopic data further might not contain information about the symmetry of the pulse in time domain or a chirp. For instance, the missing spectral phase contains information on whether a certain pulse feature such as an exponential decay is trailing or leading.

For such systems, including, e.g. FELs, real-time characterization of the pulse width and pulse shape in the time domain is essential. Many facilities monitor the pulse shape at the laser cavity, for instance by spectroscopic techniques. However, the THz pulses have to be guided to the experimental site, often several 10 m away. This gives rise to (frequency-dependent) attenuation losses, dispersion in waveguiding structures and possibly water vapor absorption. For experiments where the pulse duration and pulse shape are critical, monitoring the pulse shape as close as possible to the actual experiment drastically reduces experimental errors. Therefore, a compact detector is needed in contrast to a bulky spectrometer to be able to record the pulse shape. For pump-probe experiments, the timing between the two THz pulses or a near-infrared and

Manuscript received September 14^{th}, 2018. This work was supported by the Deutsche Forschungsgemeinschaft, Project PR1413/2-1 (LA-FET). (Corresponding author: Stefan Regensburger.)

S. Regensburger, and S. Preu are with Technische Universität Darmstadt, Germany. (e-mail: regensburger@imp.tu-darmstadt.de)

S. Winnerl, and J. M. Klopf are with the Helmholtz Zentrum Dresden-Rossendorf, Germany.

H. Lu is with the University of Nanjing, China.

A. C. Gossard is with the University of California, Santa Barbara, USA.

a THz pulse is essential. We have demonstrated that a large-area FET (LA-FET) [12], [13] can record the timing between two pulses close to real-time with a temporal resolution in the range of a few 10 ps, limited by measurement electronics and wiring.

The LA-FET is based on an antenna-less concept, where many FETs are all connected in parallel and the THz power is coupled directly to the channel and the ohmic contacts. LA-FETs feature a high damage threshold ($> 65\,\mathrm{kW}$), a large dynamic range, are ultra-fast, and do not show antenna resonances over an extreme bandwidth from 0.1 to 22 THz [12]. Therefore they are ideally suited for detection of ultra-short and high power THz pulses. The single FETs act as Hertzian dipoles, therefore the antenna resistivity and responsivity is lower as compared with a regular antenna and the devices show a roll-off towards higher frequencies.

In contrast to LA-FETs, in antenna coupled FETs (A-FETs), the THz power couples to a lumped element FET with μm dimensions with the aid of an antenna. The antenna radiation resistance is much larger than the effective radiation resistance of a LA-FET [14] leading to an increase in responsivity and therefore also lower NEP. While the large area of LA-FETs simplifies handling in the experiment, A-FETs are better suited for low THz intensities, such as in table-top applications with sub μW power levels. With broadband antennas large bandwidths have also been demonstrated for single A-FETs [15].

In this paper we demonstrate pulse width and pulse shape characterization with a LA-FET as well as an A-FET. We further demonstrate that the recorded pulse widths and pulse shape allow for direct extraction of the cavity detuning parameter for the FEL generating the THz pulse. We propose a refined approach to describe the temporal pulse shape of FELs and compare the pulse width with that obtained from spectroscopic data.

II. Experimental Setup

In this paper, the shape of THz pulses generated by the free-electron laser FELBE at the Helmholtz-Zentrum Dresden-Rossendorf is studied. In a FEL tunable radiation is generated by relativistic electrons in an undulator that is placed in a resonator cavity. The electron beam energy, period of the undulator and B-field strength of the undulator mainly determine the central frequency of the emitted radiation. The number of optical cycles is equal to the number of undulator periods, if the overlap between electron bunches and optical pulse is ideal. In the present experiments, the undulator and electron bunch parameters were optimized for a specific FEL frequency and only the cavity length was tuned by a certain length ΔL with respect to the optimum working point. Cavity detuning only slightly shifts the center frequency f_0 in the range of a few GHz but strongly alters the pulse shape. While at the optimum working point, the FEL pulse features an almost perfect Gaussian shape, a strongly detuned cavity $\Delta L \ll 0$ leads to an exponential rising edge of the FEL pulse, $p(t)$ [16], [17]. Unlike causal decay processes the leading edge is exponential, not the trailing one. In every round trip of the pulse in a ΔL shorter cavity, the leading edge of the pulse is arriving $\Delta t = 2\Delta L/c$ too early, not achieving gain in the undulator. The leading edge is therefore attenuated exponentially in each round trip, such that the rising edge of the pulse shows an exponential shape $\sim \exp(tc\alpha/2\Delta L)$, with c the speed of light. The (unitless) constant α corresponds to the loss in the cavity. The exponential constant of the rising edge can be evaluated to $\tau = 2\Delta L/\alpha c$. The highest THz power is usually extracted for a slightly negative cavity detuning $\Delta L \approx -0.2\lambda$ [18]. The cavity detuning compensates the lag of the electron bunch which is slightly slower than the speed of light, also called slippage effect. In lack of an absolute value, we denote in the following the relative cavity detuning with an offset, $\Delta L = \Delta L' + L_0$, where L_0 is close to maximum power.

The repetition rate of the THz pulses is 13 MHz. The THz beam is focused onto the FETs by a parabolic mirror. The THz beam is coupled through the substrate to the antenna coupled FET. A hyper-hemispherical silicon lens is used to increase the numerical aperture. For the LA-FET with $1 \times 1\,\mathrm{mm}^2$ active area the radiation is coupled from the air side. A horn with an aperture of 1.5 mm shields the wiring of the FET from undesired incoupling [19]. The device parameters of the LA-FET and the A-FET are compared in table I. The high electron mobility transistors (HEMTs) were epitactically grown featuring a 2-dimensional electron gas (2DEG) with very small barrier width d_{ch}. The channel is remotely doped with a silicon (Si) delta doping, leading to large electron mobilities at room-temperature [15]. For both devices, wires with a length in the range of $\sim$ 1 mm connect source and drain pads to an SMA connector. The IF path continues with a coaxial cable with 3.5 mm connectors, which feeds the signal through a large bandwidth bias-

TABLE I
Parameters of the measured FETs, where L_G is the gate length, L_{SD} the channel length, N the number of parallel connected FETs, W the width of the FETs, μ the electron mobility, n the charge carrier density, and d_{ch} the channel depth.

FET	L_G (μm)	L_{SD} (μm)	N	W (μm)	μ ($\frac{\mathrm{cm}^2}{\mathrm{Vs}}$)	n ($\frac{10^{11}}{\mathrm{cm}^2}$)	d_{ch} nm
LA-FET	3	12	48	1000	4323	1.8	15
A-FET	1.2	3.8	1	30	5750	7.1	30

tee (picosecond 5542) to a 30 GHz sampling oscilloscope (Tektronix 80E08 on DSA8200). Each device is packaged in a metal case for effective shielding from undesired noise into the large bandwidth IF signal path. For additional noise reduction, we average 100 time traces with the oscilloscope in this study. If necessary, the FET detectors can also be used for THz single-shot measurements. The responsivity of the A-FET is 5 mV/W, the responsivity of the LA-FET is 0.03 mV/W, both for the unsaturated regime of the FETs at optimum biasing conditions at 2.0 THz for the longest pulse. The responsivity decreases for shorter pulses (wider spectra) due to the limited IF bandwidth that attenuates high frequency parts the pulse. The measurements were carried out with a low THz power to obtain a rectified voltage in the same range for the FETs in order to avoid effects from saturation in the FETs. The FEL pulses were therefore attenuated with discrete elements depending on the cavity length dependent power from the FEL. The length and shape of the FEL pulse is tuned by changing the cavity length, L. A grating spectrometer records the power spectrum $\hat{p}(f)$ of the pulse for each FEL cavity length. The pulse width in the time domain is measured with both the LA-FET and A-FET for a range of gate biases.

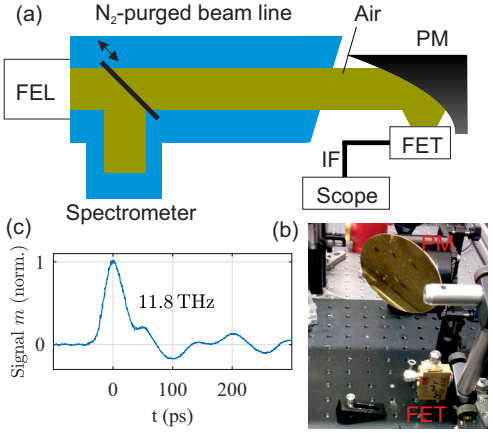

Fig. 1. (a) Schematic of the THz beam line with parabolic mirror (PM) for focussing on the FET (not to scale). (b) Picture of the setup with the packaged FET and the PM. (c) Measured impulse response of the A-FET with very short THz pulse length at 11.8 THz with a Gaussian width of 14 ps.

A simplified schematic of the beam line is shown in Fig. 1 (a). The length of the N_2-purged beamline after the spectrometer is $\approx$ 22 m. The length between the N_2-purged beam line and the FET in air is $\approx$ 3.3 m. Fig. 1 (b) shows a picture of the packaged FET detector with a parabolic mirror for focusing. Fig. 1 (c) shows the impulse response of the A-FET at 11.8 THz. The impulse response of the FET shows a Gaussian shape. The negative peak and the ringing is due to reflections in the IF-path.

III. Theory

The state of the art approach to model the FEL pulse, $p(t)$, from a detuned cavity is a piecewise defined function with an exponential rising edge and a Gaussian trailing edge, yielding a discontinuous differentiable function at the joint $t = 0$ and strong deviations from the measured pulses around the peak position, $t = 0$ [17]. An evaluation of the piecewise defined function is presented in the appendix. We also use to this model to evaluate the experimentally obtained data and compare it to the description derived in the following. We refine the piecewise defined approach with a more physical one by modeling the pulse as a convolution of a Gaussian and a rising exponential edge. This avoids any discontinuity in the derivative and further allows to describe the measured pulses directly at the peak position. Further also rising edges with a combination of Gaussian and exponential behavior for very weak cavity detunings can be modeled very well with this approach. The intensity of the THz pulse, $p(t)$ reads then

$$\begin{aligned} p(t) = &\quad p_0 \left(\exp(-t^2/2\sigma^2) * (H(-t)\exp(t/\tau))\right) \\ = &\quad p_0 \left(G_\sigma(t) * X_\tau(t)\right), \end{aligned} \tag{1}$$

where "*" denotes the convolution operator, the Gaussian part of the pulse is represented by $G_\sigma(t) = \exp(-t^2/[2\sigma^2])$ and the exponential rise is given by $X_\tau(t) = H(-t)\exp(t/\tau)$, with $H(t)$ the Heaviside step function. For the limit of no exponential broadening $\tau \to 0$, a Gaussian shape is obtained for $p(t)$, as it is expected for very weak cavity detuning $\Delta L \approx 0$. In order to compare and cross-reference the measured pulse shape to spectroscopic information on the pulse, we need to perform a Fourier transform on the field of the pulse. The envelope of the electrical field can be obtained as $E_0 \sim \sqrt{p(t)}$. Unfortunately, there is no simple Fourier transform of $\sqrt{p(t)}$ as the square root and the convolution operator do not commute. However, it can be shown that for the chosen functions $G_\sigma(t)$ and $X_\tau(t)$, the pulse $p(t)$ can be very well approximated by

$$p(t) = p_0 \left(G_\sigma(t) * X_\tau(t)\right) \approx p_0 \left(G_{\sqrt{2}\bar{\sigma}}(t) * X_{2\bar{\tau}}(t)\right)^2, \tag{2}$$

with $\sigma/\bar{\sigma} = 1.0$ for an (almost) Gaussian pulse with $\tau \ll \sigma$ while $\sigma/\bar{\sigma} \approx 1.2$ and $\tau/\bar{\tau} \approx 1.0$ for $\tau \gg \sigma$. For the pulses described in this work, the best approxmation is obtained for parameters in the range of $\tau/\bar{\tau} \approx 1.03$ and $\sigma/\bar{\sigma} \approx 1.1$. The maximum deviation of the pulse in the time domain is in the range of 0.5%, i.e. smaller than the experimental noise. The approximation is evaluated in the appendix in Fig. 6. The envelope of the field $E(t)$

can therefore also be well described by a convolution of a Gaussian function with temporal width of $\sqrt{2}\bar{\sigma}$ and an exponential rise with a time constant $2\bar{\tau}$. Eq. 1 only considers the pulse envelope measured by the FET. The oscillation frequency is not resolved by the envelope measurement. For comparison with spectroscopic data, the oscillation can be added by the factor $\exp(2\pi i f_0)$. It can either be taken from spectroscopic data or measured on-site with an autocorrelation measurement [6]. In general, there is usually no need for measuring f_0 at the experimental site because there are no severely dispersive elements in the beam line that could cause a drastic shift of the FEL frequency and the FEL frequency obtained by spectroscopy at the FEL is sufficiently accurate. The resulting electrical field, $E(t)$, becomes then

$$E(t) = E_0 \left(G_{\sqrt{2}\bar{\sigma}}(t) * X_{2\bar{\tau}}(t)\right) \exp(2\pi i f_0). \quad (3)$$

The spectrum of the electrical field is obtained through Fourier transformation:

$$\hat{E}(f) = \hat{E}_0 G_{(2\pi\sqrt{2}\bar{\sigma})^{-1}}(f - f_0) \cdot \frac{2\bar{\tau}}{1 - 4\pi i \bar{\tau}(f - f_0)}, \quad (4)$$

where we replaced $\omega = 2\pi f$. For simplicity, functions with a hat denote respective quantities in the frequency domain. The power spectrum of the pulse required for comparison with spectroscopic data is then given by

$$\hat{p}(f) = \hat{p}_0 G_{(4\pi\bar{\sigma})^{-1}}(f - f_0) \cdot L_{2\bar{\tau}}(f - f_0), \quad (5)$$

where $L_{2\bar{\tau}} = \frac{(2\bar{\tau})^2}{1+(4\pi\bar{\tau}(f-f_0))^2}$ is the Lorentz-function. The data obtained by the spectrometer measurement is fitted with Eq. 5 in order to determine the Gaussian and exponential widths, σ, and τ, respectively for comparison with the time traces recoded by the FETs.

For an ideal time domain envelope detector, also the reverse direction is possible, namely a comparison of the spectrum obtained from Eq. 5 by the Fourier transformation of a captured pulse in the time domain to that of the envelope of the spectrum obtained with a spectrometer. Since the time domain envelope detector does not resolve the oscillation at f_0, the pulse will be mapped to DC, i.e. the frequency in Eq. 5 must be replaced by $f - f_0 \to f$.

A realistic detector, however, bears some disadvantages. In general, a THz pulse is rectified applying a quadratic non-linear process on the input THz pulse $p(t)$ that is subsequently recorded with read-out electronics. The recorded pulse, $m(t)$, is therefore a convolution of the intensity of the input pulse, $p(t)$, with the transfer function of the rectifier, $r(t)$, and the transfer function of the measurement electronics, $IF(t)$,

$$m(t) = p(t) * r(t) * IF(t) = m_0 G_\sigma(t) * X_\tau(t) * r(t) * IF(t). \quad (6)$$

The functions $r(t)$ and $IF(t)$ take frequency-dependent losses and phase shifts into account, e.g. due to finite response times resulting in a low pass behavior. Both $r(t)$ and $IF(t)$ will temporally broaden the pulse and may cloak features of the pulse if the pulse duration is shorter than the time constants of $r(t)$ or $IF(t)$. The convolution $r(t) * IF(t) = IF_{eff}(t)$ can be considered as an effective post detection filter function. In the case of FELBE, typical THz pulse durations are in the range of 1-30 ps. The authors in ref. [20] calculated a FET detector time constant $< 2\,\text{ps}$ for gate biases U_{GS} and electron mobilities, μ, used in this study.

$IF(t)$ summarizes (frequency-dependent) losses within the intermediate frequency (IF) detection chain including the 30 GHz oscilloscope, wiring and cable losses. The oscilloscope response time is in the range of $\sigma_{scope} = 7$ ps, for the approximation of a Gaussian behavior from the specified rise time. RF losses by SMA cables further increase the IF time constant. It can therefore be considered (much) larger than the FET time constant and therefore dominates the temporal broadening. In this case, $IF(t)$ can be estimated from a measurement of the impulse response of the system using a pulse $p(t)$ being very short in comparison to the filter time constant of $IF(t)$.

In order to determine the function $IF_{eff}(t)$ we record a pulse at 11.8 THz that features a very short pulse duration of $\sigma_s = 2.0$ ps, determined from the measured spectroscopic data. It is known that the pulses are almost chirp-free, therefore allowing to assume that the pulse duration obtained from a Fourier transformation of the spectroscopic data indeed is the Heisenberg-Gabor limited temporal pulse width. The pulse detected by the A-FET is shown in Fig. 1 (c) for a gate bias of $-0.3\,\text{V}$. The obtained time domain trace is in very good approximation a Gaussian function of width $\sigma_m = 11.4 \pm 0.3$ ps and 14.2 ± 0.3 ps and vanishing exponential part for both LA-FET and A-FET, respectively. As the product of two Gaussian functions (i.e. $\hat{p}(f)$ and $\hat{IF}_{eff}(f)$) as well as the convolution of these functions (i.e. $p(t)$ and $IF_{eff}(t)$) yield again Gaussian functions, we conclude that the IF filter function can be well described by a Gaussian function of temporal width $\sigma_{IF,eff} = \sqrt{\sigma_m^2 - \sigma_s^2} = 11.2 \pm 0.3$ ps and 14.0 ± 0.3 ps for the LA-FET and A-FET, respectively. For any parameter combination of σ and τ, the recorded pulse in the time domain with the FETs and post detection electronics then reduces to

$$m(t) = m_0 G_{\sigma_m}(t) * X_{\tau_m}(t), \quad (7)$$

with the measured Gaussian width of $\sigma_m = \sqrt{\sigma^2 + \sigma_{IF,eff}^2}$ and exponential width $\tau_m = \tau$. Interestingly, the exponential rise time does not seem to

be affected by the low-pass behavior of the IF path. Therefore, time constants below the rise time of the oscilloscope can indeed be resolved.

IV. Results

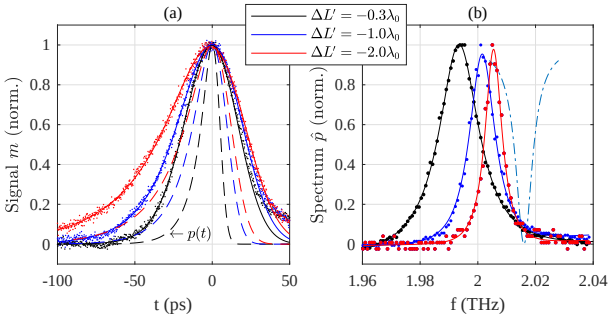

Fig. 2. (a) Rectified THz signal from the A-FET vs. time for three different THz pulses at $U_{GS} = 0$ V. The time t = 0 ps is defined as the (positive) peak position of $m(t)$. The amplitudes of the pulses are normalized. Points: recorded time domain data, solid lines: fitted pulse shape according to Eq. 7. Dashed lines: calculated time domain traces according to Eq. 1 from fits to the spectra obtained with the grating spectrometer with Eq. 5 in the same color, respectively. (b) Spectra recorded by the grating spectrometer of the corresponding THz pulses for the three different values of cavity detuning for temporal pulse broadening. The dashed dotted line represents potential transmission losses due to a waterline close to the spectra (not to scale). Only the recorded time domain traces, $m(t)$, are affected as the grating spectrometer is purged with dry nitrogen (c.f. Fig. 1).

The recorded data with both FETs show some ringing as depicted in Fig. 1 (c). This ringing is largely due to reflections by impedance mismatch in the post detection path and the wiring. The reflections start perturbing the signal a few 10 ps after the main peak as they experience a temporal delay upon reflection. The rising edge as well as the first few 10 ps after the main peak are considered reflection-free. The recorded pulses, $m(t)$, were therefore fitted with Eq. 7 in the time domain till the point where the amplitude decreased to 80% after the peak in case of the LA-FET. The A-FET shows less ringing, potentially attributed to improved wiring of a lumped element device, allowing to extend the fitting to 20% - 80% amplitude of the falling edge after the main pulse. For better comparison, all data were fitted to 80% amplitude of the falling edge, however, Fig. 2 (a) shows that there is even good agreement down to 20% of the falling edge for the A-FET. The data are recorded at an FEL frequency of 2.0±0.03 THz.

Eq. 5 and Eq. 7 excellently describe both the measured time traces $m(t)$ and measured spectra $\hat{p}(f)$ for the investigated FEL relative cavity detuning from $\Delta L' = -0.3\,\lambda_0$ with a pure Gaussian shape to $\Delta L' = -2.0\,\lambda_0$ with a pronounced exponential rising edge and therefore a strongly asymmetric shape. For the measured spectrum at $\Delta L' = 0$ (not shown), there is a shoulder in the spectra not being described Eq. 5, but the measured time traces $m(t)$ are still excellently described by Eq. 7 featuring a Gaussian shape and a vanishing exponential broadening $\tau_m \to 0$. For the fit of the spectra, $\hat{p}(f)$, we account for a faint linear ($\sim f$) background. Both the measured time traces $m(t)$ and the spectra $\hat{p}(f)$ are normalized and shown in Fig. 2 (a) and (b) respectively. We note, that the signal to noise ratio of the spectroscopic data is about an order of magnitude lower, leading to larger fit errors.

The measured pulses, $m(t)$, in Fig. 2 (a), shown as points, are fitted with Eq. 1 to obtain the measured pulse width, σ_m, and the exponential broadening, τ_m. The parameters $\bar{\sigma}_s$ and $\bar{\tau}_s$ of the (ideal) THz time domain trace, $p(t)$, are obtained by fitting the spectral data $\hat{p}(f)$ with Eq. 5 in the frequency domain. The time domain parameters σ_s and τ_s are then calculated by substituting these values into Eq. 2, assuming no further broadening e.g. by a chirp which cannot be evaluated due to the lack of spectral phase information. The dashed lines represent the THz pulses, $p(t)$, calculated from the fitted spectra. The broadening of the measured pulses, $m(t)$, as compared to the THz pulses $p(t)$ represents the broadening due to the measurement path $IF(t)$ and the rectification $r(t)$.

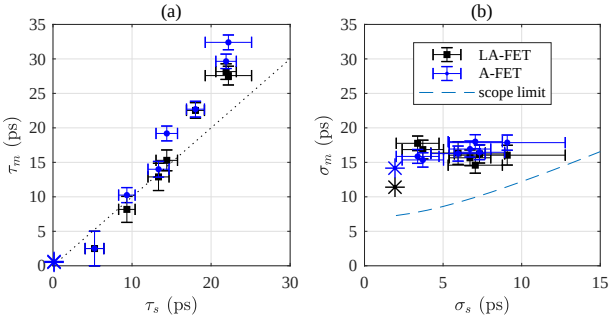

Fig. 3. Measured pulse widths for the LA-FET and the A-FET vs THz pulse width extracted from the spectra $\hat{p}(f)$ at 2.0 THz for $U_{GS} = 0$ V. The THz pulse width is changed through detuning of the FEL cavity from $\Delta L' = 0.0\lambda_0$ to $-2.0\lambda_0$ (a) Exponential Broadening τ_m vs τ_s. (b) Gaussian width σ_m vs σ_s. The star symbols display the impulse response measurement at 11.8 THz with a very short pulse width for $U_{GS} = -0.3$ V and -0.5 V for the A-FET and LA-FET respectively.

Fig. 3 (a) depicts the exponential rise time obtained from the time domain traces recorded with both FETs vs. the rise time calculated from the spectra, τ_s. The measured exponential broadening τ_m shows a linear behavior in comparison with the τ_s from $\hat{p}(f)$ with apparently only minor or no limitations by $IF(t)$ and $r(t)$. The dotted line is a guide to the eye for a perfect 1:1 correspondence. The star symbols display the resulting pulse width of the short 11.8 THz pulse for reference. However, τ_m increases stronger than expected for very long τ resulting in values $\tau_m > \tau_s$. The time traces $m(t)$

are measured after a transmission path of the THz pulses in air while the spectra, $\hat{p}(f)$ are recorded in a dry nitrogen atmosphere. Though care was taken to use a FEL frequency that does not coincide with any water lines, the pulses sightly shift with cavity detuning. Spectrally narrower pulses, i.e. pulses with larger detuning appear at slightly higher mean frequencies and start touching a water line at 2.016 THz as shown in Fig. 2 (b) (dashed dotted line). Losses by water vapor absorption within the path between the N_2 purged beam guide and the actual experiment of $\approx$ 3.3 m, reduce the spectral width of the pulse and may therefore be responsible for excessive temporal broadening at large cavity detunings.

The Gaussian part σ_m in Fig. 3 (b) does not show any noticeable dependence on pulse widths σ_s except for the shortest pulse recorded at 11.8 THz, displayed as stars where the LA-FET shows a slightly faster detection with $\sigma_m \approx \sigma_{IF_{eff}} \approx 11$ ps as compared with the A-FET with $\sigma_m \approx \sigma_{IF_{eff}} \approx 14$ ps for a FEL pulse width of $\sigma_s = 2$ ps. The data include the limitations by $IF(t)$ and $r(t)$. The dashed line is the theoretical limit of the used oscilloscope, $\sigma_m^{theo} = \sqrt{\sigma^2 + \sigma_{IF}^2}$, where $\sigma_{IF} = 7$ ps is fitted to the rise time of the oscilloscope. This lower limit assumes only a low-pass behavior of the oscilloscope and neglects any influence by cables or the FETs, $r(t)$. From the difference to the oscilloscope limit, we can estimate the the time constant of the low-pass filter due to cabling and $r(t)$ to ≈8.5 ps which can be considered as an upper limit of the response time of the FETs.

In agreement with Eq. 7, broadening due to $r(t)$ and $IF(t)$ does not show any effect on τ_m. The obtained values of τ_m can therefore be used to calculate the cavity loss factor and the cavity detuning, ΔL, of the FEL. The exponential broadening is linked to the cavity detuning by [17]

$$\tau = \frac{2}{\alpha c}\Delta L' + \frac{2}{\alpha c}L_0. \qquad (8)$$

Fig. 4 compares the extracted exponential broadening τ_m for the measured time traces and τ_s from the spectroscopic data for both the convolution ansatz in Eq. 5 and the piecewise ansatz of Eq. 10 vs. cavity detuning. Generally speaking, the spectrometer data show slightly shorter rise times, potentially attributed to beam guiding in an N_2 atmosphere while the FET measurements were carried out in normal air. As discussed above, particularly measurements with larger detunings are affected by water vapor absorption where the deviations to the spectroscopic data are largest. At low cavity detunings, $|\Delta L'| \leq \lambda$, however, the agreement between spectroscopic data and the convolution approach is excellent. Over the whole investigated range of detunings, the piecewise ansatz (Eq. 9) yields larger rise times than the convolution

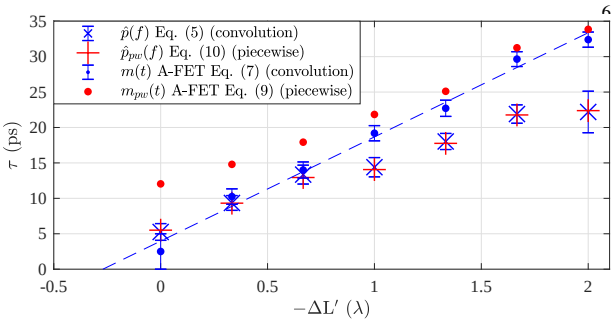

Fig. 4. Exponential broadening τ vs normalized cavity detuning $\Delta L'$ with comparison of convolution and piecewise ansatz (Appendix, Eq. 9). For the rise times τ_s derived from the spectroscopic data, $\hat{p}(f)$, the two different approaches show a very similar behavior (blue and red crosses). For the rise times determined from the FET measurements in the time domain, τ_m, the convolution approach yields $\Delta L'$ much better agreement with the spectroscopic data, in particular at very low detuning, i.e. very short exponential rise times. The dashed line shows the fit for the measured time domain traces with the convolution approach.

approach from Eq. 7 and larger deviations from the spectroscopic data, in particular at small detunings. This deviation can be accounted to the missing capability of this ansatz to seperate the IF-limitations. Only at very large cavity detuning $\Delta L' \rightarrow -2\lambda$ the piecewise ansatz approaches the values from the convolution ansatz. We therefore conclude that the convolution ansatz presented here is superior for describing the FEL pulse as compared to the piecewise definition found in the literature.

With the convolution approach for A-FET and LA-FET a cavity loss of $\alpha = 0.07$ is obtained from the slope of the graphs in Fig. 4, which compares well to the simulated cavity loss of $\alpha = 0.05$. From the spectrometer data, $\hat{p}(f)$, the extracted cavity loss of $\alpha \approx 0.11$ is higher. This deviation can potentially be attributed to the spectral narrowing/temporal broadening by water vapor absorption as discussed previously in conjunction with the discussion of Fig. 3 a).

The ordinate at $\Delta L' \rightarrow 0$ allows to determine the absolute cavity detuning ΔL to $L_0 = -0.3\lambda$ from the time traces with the convolution approach. From the spectrum measurements we obtain a value of $L_0 = -0.6\lambda$ for the absolute cavity detuning. These values compare well with the slippage length of -0.2λ experimentally found for power-optimized detuning in saturation [18] and the theoretical value of $-\lambda$ for non-saturated operation.
Finally, we use the temporal broadening of the FEL by cavity detuning to estimate the response time of the FETs with respect to gate bias.

Fig. 5 shows the dependence of the measured pulses $m(t)$ from the gate bias U_{GS} for the LA-FET and A-FET for two exemplary THz pulse widths. For the

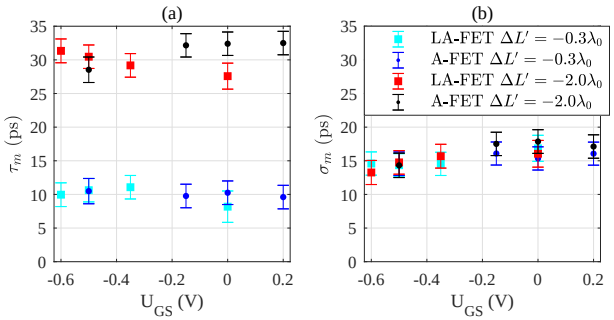

Fig. 5. Measured pulse width vs. gate bias U_{GS} for the LA-FET and the lumped element FET. (a) Exponential Broadening τ_m vs U_{GS}. (b) Gaussian width σ_m vs U_{GS}. The gate bias does not show a significant influence on the exponential broadening τ_m, but a trend to smaller Gaussian widths σ_m for more negative gate bias U_{GS}.

exponential broadening (Fig. 5 (a)) no clear dependence is found within the measurement error, $\Delta\tau_m = \pm 1$ ps, in agreement with Eq. 7: the exponential term is not affected by Gaussian broadening caused by the IF path and $r(t)$. According to the literature, the response time of the rectification process, $r(t)$, is expected to increase for U_{GS} closer to the threshold bias [20]. Contrary, the Gaussian width, σ_m, shows a slight trend to smaller values and thus faster detection speed for smaller gate biases U_{GS}. The reduction of the Gaussian width from about 16 ps at $U_{GS} = 0\,V$ to ≈ 14 ps at $U_{GS} = -0.6\,V$ at a threshold bias of $U_{th} \approx -0.4$ V (-0.5 V) for the LA-FET (A-FET) is only slightly above the measurement error that we estimated to $\Delta\sigma_m = \pm 1$ ps. While we cannot tell apart any change in $r(t)$ and $IF(t)$, the reduction of σ_m could also be accounted to a dependence of $IF(t)$ on U_{GS}. The gate bias, U_{GS}, changes the impedance of the FET, therefore also the reflection in the IF-wiring due to an impedance mismatch between the FET and the coaxial cable. For the A-FET the amplitude of the negative after-pulse decreases with more positive gate bias U_{GS}. An increased gate bias U_{GS} leads to a decrease in channel resistance of the FET. For the lumped element A-FET the source drain resistance does not drop below 400 Ohms. For the LA-FET the amplitude of the negative after-pulse is minimum for $U_{GS} = -0.35$ V, where the source drain resistance is close to 50 Ohms. For higher or lower gate biases the amplitude increases in agreement with impedance-matching. As the change in σ_m is only $\lessapprox 3$ ps despite a large range of investigated gate biases U_{GS}, we conclude that the IF-path $IF(t)$ is dominating the observed broadening of the measured pulse in this study.

V. Conclusion

Both the LA-FET and the A-FET are excellent real-time detectors for Terahertz pulses with an IF-bandwidth of tens of GHz, currently only limited by the speed of post detection electronics. While very fast, A-FETs are more sensitive than LA-FETs. They are therefore also suited for low THz power experiments, as well as for broadband THz communication.

LA-FETs are much more robust than A-FETs and fea-ture a large linearity range, high damage threshold and a well-defined frequency dependence over an extreme bandwidth as we have shown previously [12]. They are therefore well suited for applications at high power THz facilities. Future devices of both types can be produced with an improved IF-path and wiring with less impedance mismatch for a further decrease of ringing after the main pulse and improved IF performance with larger bandwidth. Due to bandwidth limitations by wiring and the IF post detection electronics, the presented results only allow for defining an upper limit for the response time of the FETs of ≈ 8.5 ps.

In order to demonstrate the high speed of the FETs, we experimentally studied THz pulses from a FEL. With the refined ansatz for the measured FEL pulses as a convolution of a Gaussian and an exponential function, we can extract the Gaussian width, and the exponential rise time much more precise than with the commonly used piecewise composed description. It further allows to include the low-pass behavior of the IF electronics and wiring in a simple way. The exponential rise time obtained by the FET measurements is very close to that of obtained by a spectrometer, despite the fact that the values are very close to or even below the resolution limit of the oscilloscope used for read-out of the FET signals. The minimum detectable exponential rise time is about $\lessapprox 5$ ps, despite a limitation in the IF-path low pass behavior with a time constant of ≈ 11 ps and ≈ 14 ps for the LA-FET and A-FET, respectively. The exponential rise time extracted from the measurements with the FET detectors allows to deduce the cavity detuning parameter of the FEL. We therefore conclude that the description of the FEL pulse by a convolution is superior to a piecewise approach, particularly in the limit of zero exponential broadening.

VI. Appendix

For comparison of this study to the literature [17] the piecewise combination of a exponential rising and Gaussian falling edge is defined as

$$p_{pw}(t) = p_0 \cdot \begin{cases} \exp(+t/\tau) & \text{for } t < 0 \\ \exp(-t^2/2\sigma^2) & \text{for } t \geq 0 \end{cases}. \quad (9)$$

By Fourier transformation of the respective field-quantity ($\sqrt{p_{pw}(t)}\exp(2\pi i f_0)$) the intensity spectrum $\hat{p}_{pw}(f)$ is

obtained as follows:

$$\hat{p}_{pw}(f) = \hat{p_0} \left| \frac{\tau/2 - 2\pi\tau i\tilde{f}}{1/4 + 4\pi^2\tau^2\tilde{f}^2} + \sigma\sqrt{\pi}e^{-4\pi^2\sigma^2\tilde{f}^2} + 2\tau i\,\mathrm{D}(2\pi\sigma\tilde{f}) \right|^2, \quad (10)$$

where $\mathrm{D}(x)$ denotes the Dawson integral and $\tilde{f} = f - f_0$. The extracted parameters from the fit to the spectra are compared in Fig. 4 for the convolution approach and the piecewise ansatz.

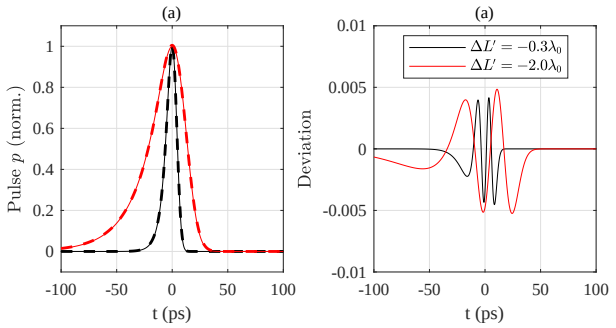

Fig. 6. (a) Comparison of the approximation for $p(t)$ from Eq. 2 for $G_\sigma * X_\tau$ (dashed line) and $(G_{\sqrt{2}\bar{\sigma}} * X_{2\bar{\tau}})^2$ (solid line) for two different settings $\Delta L'$ of the FEL. The lines show excellent agreement. (b) Absolute deviation of the approximation for each of two FEL settings, $\Delta L'$, shown in (a).

In Fig. 6 we review the approximation of Eq. 2 for $G_\sigma * X_\tau$ and $(G_{\sqrt{2}\bar{\sigma}} * X_{2\bar{\tau}})^2$, showing a maximum deviation in the range of 0.5% which is lower than the measurement noise.

In order to ascertain that the exponential rise time is indeed not affected by Gaussian broadening, we further simulated the theoretical fitting accuracy of the detection process of Eq. 7 by adding simulated noise to achieve a signal to noise ratio comparable to the measurements. For the Gaussian broadening a value of $\sigma_m = 16\,\mathrm{ps}$ in the same range as the measurements was used. We repeated the fitting 1000 times, adding random noise and comparing the parameters of the resulting fits. For an exponential broadening of $\tau_m \geq 4\,\mathrm{ps}$ the fitting error in τ and σ (distribution of the resulting fit parameters) is smaller than 0.5 ps, despite the assumed Gaussian broadening of $\sigma_m = 16\,\mathrm{ps}$. We further note, that for an exponential broadening of $\tau_m \lessapprox 1\,\mathrm{ps}$, the obtained curve shape is very close to or within the numerical precision even identical to a Gaussian shape with $\sigma_m = 16\,\mathrm{ps}$. For an exponential broadening of $\tau_m \lessapprox 3\,\mathrm{ps}$, the fitting routine also shows numerical instabilities, due to the small difference in the resulting function from a pure Gaussian shape. We therefore conclude that the theoretically minimum detectable *exponential* rise time is even smaller than found in the experiment and more than a factor of four smaller than the *Gaussian* time constant. The Gaussian shape of the impulse response justifies that the influence from $IF_{eff}(t)$ is included in the measured Gaussian width σ_m and not in the measured exponential broadening τ_m.

Acknowledgment

We are grateful to P. Michel and the FELBE team for their dedicated support. Details from previous FELBE simulations and commissioning were generously provided by Ulf Lehnert.

References

[1] M. Dyakonov and M. Shur, "Detection, mixing, and frequency multiplication of terahertz radiation by two-dimensional electronic fluid," *IEEE Transactions on Electron Devices*, vol. 43, no. 3, pp. 380–387, mar 1996.

[2] J. Grzyb and U. Pfeiffer, "THz Direct Detector and Heterodyne Receiver Arrays in Silicon Nanoscale Technologies," *Journal of Infrared, Millimeter, and Terahertz Waves*, vol. 36, no. 10, pp. 998–1032, oct 2015.

[3] M. Bauer, R. Venckevičius, I. Kašalynas, S. Boppel, M. Mundt, L. Minkevičius, A. Lisauskas, G. Valušis, V. Krozer, and H. G. Roskos, "Antenna-coupled field-effect transistors for multispectral terahertz imaging up to 4.25 THz." *Optics express*, vol. 22, no. 16, pp. 19 235–41, aug 2014.

[4] T. Nagatsuma, "Breakthroughs in Photonics 2013: THz Communications Based on Photonics," *IEEE Photonics Journal*, vol. 6, no. 2, pp. 1–5, apr 2014.

[5] F. Rettich, N. Vieweg, O. Cojocari, and A. Deninger, "Field Intensity Detection of Individual Terahertz Pulses at 80 MHz Repetition Rate," *Journal of Infrared, Millimeter, and Terahertz Waves*, vol. 36, no. 7, pp. 607–612, jul 2015.

[6] S. Preu, M. Mittendorff, S. Winnerl, O. Cojocari, and A. Penirschke, "THz Autocorrelators for ps Pulse Characterization Based on Schottky Diodes and Rectifying Field-Effect Transistors," *IEEE Transactions on Terahertz Science and Technology*, vol. 5, no. 6, pp. 922–929, nov 2015.

[7] A. Lisauskas, K. Ikamas, S. Massabeau, M. Bauer, D. Čibiraite, J. Matukas, J. Mangeney, M. Mittendorff, S. Winnerl, V. Krozer, and H. G. Roskos, "Field-effect transistors as electrically controllable nonlinear rectifiers for the characterization of terahertz pulses," *APL Photonics*, vol. 3, no. 5, p. 051705, may 2018.

[8] C. Fattinger and D. Grischkowsky, "Point source terahertz optics," *Applied Physics Letters*, vol. 53, no. 16, pp. 1480–1482, oct 1988.

[9] M. van Exter and D. Grischkowsky, "Characterization of an optoelectronic terahertz beam system," *IEEE Transactions on Microwave Theory and Techniques*, vol. 38, no. 11, pp. 1684–1691, 1990.

[10] Q. Wu and X. Zhang, "Free-space electro-optic sampling of terahertz beams," *Applied Physics Letters*, vol. 67, no. 24, pp. 3523–3525, dec 1995.

[11] A. Muraviev, A. Gutin, G. Rupper, S. Rudin, X. Shen, M. Yamaguchi, G. Aizin, and M. Shur, "New optical gating technique for detection of electric field waveforms with subpicosecond resolution," *Opt. Express*, vol. 24, no. 12, pp. 12 730–12 739, jun 2016.

[12] S. Regensburger, M. Mittendorff, S. Winnerl, H. Lu, A. C. Gossard, and S. Preu, "Broadband THz detection from 0.1 to 22 THz with large area field-effect transistors," *Optics express*, vol. 23, no. 16, pp. 20 732–20 742, 2015.

[13] S. Preu, M. Mittendorff, S. Winnerl, H. Lu, A. C. Gossard, and H. B. Weber, "Ultra-fast transistor-based detectors for precise timing of near infrared and THz signals." *Optics express*, vol. 21, no. 15, pp. 17 941–50, jul 2013.

[14] S. Regensburger, H. Lu, A. C. Gossard, and S. Preu, "Comparison of large area and lumped element field-effect transistors for broadband detection of Terahertz," in *International Conference on Infrared, Millimeter, and Terahertz Waves, IRMMW-THz*. IEEE, aug 2017.

[15] S. Regensburger, A. k. Mukherjee, S. Schonhuber, M. A. Kainz, S. Winnerl, J. M. Klopf, H. Lu, A. C. Gossard, K. Unterrainer, and S. Preu, "Broadband Terahertz Detection with Zero-Bias Field-Effect Transistors between 100 GHz and 11.8 THz with a Noise Equivalent Power of 250 pW/$\sqrt{Hz}$ at 0.6 THz," *IEEE Transactions on Terahertz Science and Technology*, vol. 8, no. 4, pp. 465–471, 2018.

[16] M. Teich, M. Wagner, H. Schneider, and M. Helm, "Semiconductor quantum well excitons in strong, narrowband terahertz fields," *New Journal of Physics*, vol. 15, no. 6, p. 065007, jun 2013.

[17] A. M. MacLeod, X. Yan, W. A. Gillespie, G. M. H. Knippels, D. Oepts, A. F. G. van der Meer, C. W. Rella, T. I. Smith, and H. A. Schwettman, "Formation of low time-bandwidth product, single-sided exponential optical pulses in free-electron laser oscillators," *Physical Review E*, vol. 62, no. 3, pp. 4216–4220, sep 2000.

[18] D. Jaroszynski, D. Oepts, A. Van Der Meer, P. Van Amersfoort, and W. Colson, "Consequences of short electron-beam pulses in the FELIX project," *Nuclear Instruments and Methods in Physics Research Section A: Accelerators, Spectrometers, Detectors and Associated Equipment*, vol. 296, no. 1-3, pp. 480–484, oct 1990.

[19] S. Regensburger, S. Winnerl, J. M. Klopf, H. Lu, A. C. Gossard, and S. Preu, "Investigation of parasitic coupling of THz radiation to a large area field-effect transistor," in *2017 42nd International Conference on Infrared, Millimeter, and Terahertz Waves (IRMMW-THz)*. IEEE, aug 2017.

[20] S. Rudin, G. Rupper, and M. Shur, "Ultimate response time of high electron mobility transistors," *Journal of Applied Physics*, vol. 117, no. 17, p. 174502, may 2015.

Stefan Regensburger received the B.Sc. and M.Sc. degrees in physics from the Friedrich-Alexander Universität Erlangen-Nürnberg, Erlangen, Germany, in 2011 and 2013, respectively, and is currently working toward the Ph.D. degree at the Terahertz Devices and Systems Group, Department of Electrical Engineering and Information Technology, Technische Universität Darmstadt, Darmstadt, Germany.

His research interests include field-effect transistor rectifiers and THz spectroscopy of conductive thin films.

Stephan Winnerl received the Diploma and Ph.D. degrees from the University of Regensburg, Regensburg, Germany, in 1996 and 1999, respectively.

He was with the Forschungszentrum Jülich, as a postdoctoral member for two and a half years. Since 2002, he has been with the Helmholtz- Zentrum Dresden-Rossendorf (HZDR, formerly Forschungszentrum Dresden-Rossendorf), Dresden, Germany, andwas appointed an HZDR Research Fellow in 2014. He has authored or coauthored more than 175 peer-reviewed publications. His research interests include ultrafast and nonlinear spectroscopy of semiconductor quantum structures and two-dimensional materials, in particular in the THz frequency range. Furthermore, he develops emitters and fast detectors for THz radiation.

Dr. Winnerl is a member of the German Physical Society.

J. Michael Klopf received the B.S. degree in physics from Louisiana State University, Baton Rouge, LA, USA, in 1993, and the Ph.D. degree in engineering physics from the University of Virginia, Charlottesville, VA, USA, in 2005. Before graduate school, he was with the CAMD Synchrotron Facility, as a Research Associate. In 2005, he began work with the Free Electron Laser Division, Thomas Jefferson National Accelerator Facility, first as a Postdoctoral Researcher, then as a Staff Scientist. Since 2015, he has been the FEL Beamline Scientist with the ELBE Center for High-Power Radiation Sources, Helmholtz-Zentrum Dresden-Rossendorf, Dresden, Germany. He has authored or co-authored more than 50 journal and conference publications and holds 1 U.S. patent. His research interest is focused on laser driven ultrafast dynamics in materials and applications related to FEL and accelerator physics.

Dr. J. Michael Klopf is a member of the American Physical Society and the German Physical Society.

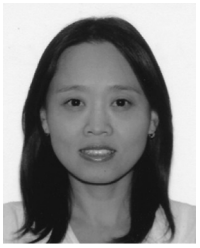

Hong Lu received the B.S. degree in chemistry from the University of Science and Technology of China, Hefei, China, and the Ph.D. degree in chemistry from the City University of New York, New York, NY, USA, in 2007, where she was focused on intersubband transitions of wide-bandgap II-VI semiconductors grown by molecular beam epitaxy (MBE).

After working as a Project Scientist with the Materials Department, University of California at Santa Barbara, Santa Barbara, CA, USA for eight years, she joined Nanjing University,Nanjing, China, where she is currently a Professor with the Department of Materials Science and Engineering, College of Engineering and Applied Sciences. She has co-authored more than 100 papers in refereed journals. Her current research interests include using and developing MBE growth techniques for synthesis of novel materials and material structures, and characterization and processing for fundamental understanding and device applications, especially heterostructures formed by semiconductors, metals, and semimetals, and their applications in optoelectronics, thermal management, and tetrahertz-based technology.

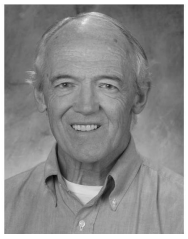

Arthur C. Gossard (LF'12) is currently a Professor of materials and electrical and computer engineering with the University of California at Santa Barbara, Santa Barbara, CA, USA. His current research interests include molecular beam epitaxy, the growth of quantum wells and super lattices, and their applications to high-performance electrical and optical devices.

Prof. Gossard is a Fellow of the American Physical Society and the American Association for the Advancement of Science,Washington, DC, USA. He is also a member of the National Academy of Engineering and the National Academy of Sciences.

Sascha Preu received the diploma degree in 2005, and the Ph.D. degree in physics (summa cum laude) from the Friedrich-Alexander Universität Erlangen-Nürnberg, Erlangen, Germany, in 2009.

From 2004 to 2010, he was with the Max Planck Institute for the Science of Light, Erlangen. From 2010 to 2011 he was with the Department of Materials and Physics, University of Santa Barbara, Santa Barbara, CA, USA. From 2011 to 2014, he worked at the Chair of Applied Physics, Universität Erlangen-Nürnberg. He is currently a Professor with the Department of Electrical Engineering and Information Technology, Technische Universität Darmstadt, Germany, leading the Terahertz Devices and Systems Group. He has authored or co-authored more than 70 journal papers and conference contributions. His research interests include the development of semiconductor based THz sources and detectors, including photomixers, photoconductors and field effect transistor rectifiers and THz systems constructed thereof. He also works on applications of THz radiation, in particular the characterization of novel THz components and materials, including graphene.